Resonant plankton patchiness induced by large-scale turbulent flow

William J. McKiver and Zoltán Neufeld
School of Mathematical Sciences and Complex and Adaptive Systems Laboratory, Dublin, Ireland
(Received 19 July 2010; published 10 January 2011)

Here we study how large-scale variability of oceanic plankton is affected by mesoscale turbulence in a spatially heterogeneous environment. We consider a phytoplankton-zooplankton (PZ) ecosystem model, with different types of zooplankton grazing functions, coupled to a turbulent flow described by the two-dimensional Navier-Stokes equations, representing large-scale horizontal transport in the ocean. We characterize the system using a dimensionless parameter, $\gamma = T_B/T_F$, which is the ratio of the ecosystem biological time scale T_B and the flow time scale T_F. Through numerical simulations, we examine how the PZ system depends on the time-scale ratio γ and find that the variance of both species changes significantly, with maximum phytoplankton variability at intermediate mixing rates. Through an analysis of the linearized population dynamics, we find an analytical solution based on the forced harmonic oscillator, which explains the behavior of the ecosystem, where there is resonance between the advection and the ecosystem predator-prey dynamics when the forcing time scales match the ecosystem time scales. We also examine the dependence of the power spectra on γ and find that the resonance behavior leads to different spectral slopes for phytoplankton and zooplankton, in agreement with observations.

DOI: 10.1103/PhysRevE.83.016303 PACS number(s): 47.27.T−, 87.23.Cc

I. INTRODUCTION

Phytoplankton species play a key role in the global carbon cycle. Their position at the bottom of the marine food chain means that all higher trophic levels, from tiny zooplankton crustaceans such as copepods to ocean giants such as the blue whale, all depend on phytoplankton in order to survive. Phytoplankton obtain energy through the process of photosynthesis (i.e., synthesizing carbohydrates from carbon dioxide and nutrients by means of sunlight), and while most individual phytoplankton cannot be seen with the naked eye, their global abundance within the ocean is so great that they account for roughly half of the total biological production on the planet [1]. In order to perform photosynthesis, phytoplankton usually resides in the uppermost layer (∼100 m) of the ocean, known as the euphotic layer, where light levels are sufficiently high for photosynthesis to occur; however, typically the nutrients that phytoplankton require often reside in deeper waters. Phytoplankton generally have limited or no swimming ability and so are at the mercy of the ocean circulation, which also affects the transport of nutrients, resulting in the complex dynamics of the entire plankton ecosystem.

Many observations of phytoplankton have revealed strong heterogeneity (patchiness) in spatial distribution over a wide range of scales [2,3]. Microscale patchiness has been observed from micrometers to centimeters [4,5], and various mechanisms for the clustering and aggregation of the microorganisms have been proposed [6–9]. Here, we focus on the large-scale variability of plankton, on scales from kilometers to several hundreds of kilometers , that is well known from ocean satellite observations. On these scales, the plankton population can be described by a continuous concentration field with its spatial distribution influenced by both physical and biological factors, the main ones being availability of light, availability of nutrients, and the advection by ocean currents. The oceanic flow responsible for the advection of plankton on scales of 1–500 km is the horizontal transport by mesoscale eddies that is qualitatively similar to two-dimensional (2D) turbulent flows, which in the enstrophy cascade regime have a characteristic structure dominated by coherent vortices [10,11]. When favorable conditions are encountered, phytoplankton can undergo a rapid population growth usually referred to as "blooms." Such heterogeneity was shown to have a strong effect on plankton productivity [12]. How the interplay between biological and physical processes controls the dynamics and spatial structure of plankton ecosystems has been studied extensively over the past decades and is still an open question.

The effect of horizontal turbulent stirring on large-scale patchiness has been examined in many previous studies (see [3] and [13] for reviews) using a number of different approaches to the problem. Some studies have focused on the analysis of the population dynamics described by the ecosystem equations [14,15], while others examined the power spectra to understand how phytoplankton and zooplankton patchiness is affected by advection at different spatial scales [16–19]. One approach taken in [20] looked at how to parametrize the role of horizontal advection relative to biological effects in a simple phytoplankton model with a spatially varying carrying-capacity field (see also [21]). The authors characterized the system in terms of a dimensionless parameter, $\gamma = T_B/T_F$, which is the ratio of the typical ecosystem biological time scales T_B (such as the inverse of the growth rate of phytoplankton) and the typical flow time scales T_F (such as the average eddy rotation period), and examined how the statistical properties of the phytoplankton depend on the time-scale ratio parameter γ. It was found that changes in the ratio of these time scales affect both the spatial structure and the total biomass (average concentration) of the plankton species and that the system can be characterized by an effective carrying capacity, which changes with γ. It was also shown that in the presence of predation (grazing) by a constant zooplankton population this type of stirring effect can produce a dramatic change in the total biomass by inducing sharp transitions (regime shifts) when γ is modified by some external factors [21].

Though these studies were performed using only a single-component phytoplankton model, nevertheless they provided a heuristic understanding of how changes in the rate of

horizontal advection can affect the average phytoplankton concentration. Here, we extend this approach using a more complex ecosystem model, a phytoplankton-zooplankton (PZ) model with an advected carrying capacity, and study how the transfer of spatial variability of the environment through the trophic levels is controlled by the biological and advective time scales. We focus particularly on possible mechanisms through which advection by the same turbulent flow can have different effects on the heterogeneity of the phytoplankton and zooplankton fields, respectively, as suggested by observations. In Sec. II, we discuss the coupled fluid-ecosystem model that we study. In Sec. III, we present the results of our numerical simulations, followed by an analysis of the equations in Sec. IV and the power spectra in Sec. V. Finally, we discuss the implications of our results in Sec. VI.

II. MODEL

Here, we consider a PZ model coupled to a carrying-capacity field and advection by a turbulent flow:

$$\frac{\partial K}{\partial t} + \mathbf{u}\cdot\nabla K = \alpha[K_b(\mathbf{x}) - K], \tag{1a}$$

$$\frac{\partial P}{\partial t} + \mathbf{u}\cdot\nabla P = rP\left(1 - \frac{P}{K}\right) - gG(P)Z, \tag{1b}$$

$$\frac{\partial Z}{\partial t} + \mathbf{u}\cdot\nabla Z = \nu gG(P)Z - \mu Z, \tag{1c}$$

where $P \equiv P(\mathbf{x},t)$, $Z \equiv Z(\mathbf{x},t)$, and $K \equiv K(\mathbf{x},t)$ are the phytoplankton, zooplankton, and carrying-capacity (maximum phytoplankton concentration attainable within that fluid parcel in the absence of grazing) concentrations respectively, r is the maximum phytoplankton growth rate, g is the grazing rate, $G(P)$ is the grazing function, ν is the grazing efficiency, μ is the zooplankton mortality rate, and $\mathbf{u}(\mathbf{x},t) = (u,v)$ is the two-dimensional horizontal flow velocity field. The carrying capacity represents the nonuniform nutrient supply (upwelling, storm surges, etc.), which is advected by the flow but has a fixed background distribution, for which we choose a simple qualitative form, $K_b(\mathbf{x}) \equiv K_0 + \delta\cos(x+y)$, as was used in previous works [16,18]. However, the results are independent of the exact form of K_b. The possible time dependence of $K_b(\mathbf{x})$ is also neglected, but this is not essential since advection by the turbulent flow generates a time-dependent carrying-capacity field, therefore introducing further time dependence in K_b does not lead to qualitatively different behavior. For the grazing function, we consider three different functional forms that have been widely used in plankton ecosystem models: (i) $G(P) = P$, (ii) $G(P) = P/(S+P)$, and (iii) $G(P) = P^2/(S^2+P^2)$, where the parameter S is the half saturation constant. For case (i), there is a linear response of predator to prey density. The cases (ii) and (iii) are the standard Holling type II and Holling type III functional forms respectively [22–25]. Holling type II models the fact that predators can only consume prey at a finite maximum rate and therefore saturation occurs when the amount of prey grows. This is also the case for Holling type III; however, at small prey density, there is a quadratic response, meaning that the predators have a low foraging efficiency at low prey density.

The flow field, $\mathbf{u}$, is obtained by solving the 2D incompressible Navier-Stokes equations with forcing and dissipation [26]:

$$\frac{\partial \zeta}{\partial t} + \mathbf{u}\cdot\nabla\zeta = F + D, \tag{2}$$

where $\zeta \equiv \partial v/\partial x - \partial u/\partial y$ is the vorticity field, which is a scalar in 2D flows, D is the dissipation, and F is the forcing. The dissipation is a combination of hyperviscosity of the form $D_{hi} = -\nu_v\nabla^8\zeta$ and linear friction, given by $D_{lo} = -\alpha\zeta$, that prevents accumulation of energy at the largest scales via the inverse cascade. The forcing is applied in spectral space at the large-scale wave number of $k_F = 10$ (i.e., at one tenth of the domain size) and has a fixed amplitude but with a random phase. This forcing inputs energy at large scales, which represents the typical size of mesoscale eddies of the order of 50 km [27]; thus our domain size corresponds to roughly 500 km in the ocean. The energy spectrum has a slope close to k^{-3} downscale of the forcing (see [20]).

Following the approach of [20], we introduce the time-scale ratio defined as the nondimensional parameter $\gamma \equiv T_B/T_F$, where T_B is the biological time scale defined as the inverse of the maximum phytoplankton growth rate (i.e., $T_B \equiv 1/r$), and T_F is the flow time scale, which is defined as $T_F = L/U$, where L is the forcing length scale $L \equiv 2\pi/k_f$ and U is the root-mean-square (rms) flow velocity. Thus, γ is given by

$$\gamma = \frac{U}{rL}, \tag{3}$$

and we can use this to write the ecosystem dynamics in dimensionless form as

$$\begin{aligned}\frac{\partial P}{\partial t} + \mathbf{u}\cdot\nabla P &= \frac{1}{\gamma}\left[P\left(1-\frac{P}{K}\right) - g'G(P)Z\right],\\ \frac{\partial Z}{\partial t} + \mathbf{u}\cdot\nabla Z &= \frac{1}{\gamma}[\nu' g' G(P)Z - \mu' Z],\end{aligned} \tag{4}$$

where the parameters have been rescaled by the growth rate r, i.e. $\mu' = \mu/r$, $g' = g/r$ etc. From now on, we drop the primes on the rescaled parameters, and they are chosen to be $g = 2$, $\nu = 0.02$, $\mu = 0.02$, $S = (2/3)K_0$, and $\alpha = 0.05$. Here, we set the characteristic flow time scale T_F to unity and vary the time-scale ratio γ.

The ecosystem equations, (IIa) and (4), are solved on a doubly periodic domain, using a semi-Lagrangian scheme with a grid resolution of 1024 squared. The advecting fluid velocity is obtained by solving Eq. (2) using the pseudospectral method. A fourth-order Runge-Kutta scheme is used for the time integration of all the equations. The plankton dynamics is solved within fluid parcels, whose motion are tracked using the midpoint method and then calculated on grid points using bicubic interpolation (see [28] and [29] for details of the semi-Lagrangian method). We do not add diffusion explicitly in our model, but some numerical diffusion is always present as a result of using interpolation in the semi-Lagrangian scheme as is discussed in [30].

In the next section, we show the results obtained by performing a number of simulations for a large range of the parameter γ. The Navier-Stokes equations are integrated until the energy reaches a statistically steady state. We then use this as the initial flow field and integrate the coupled

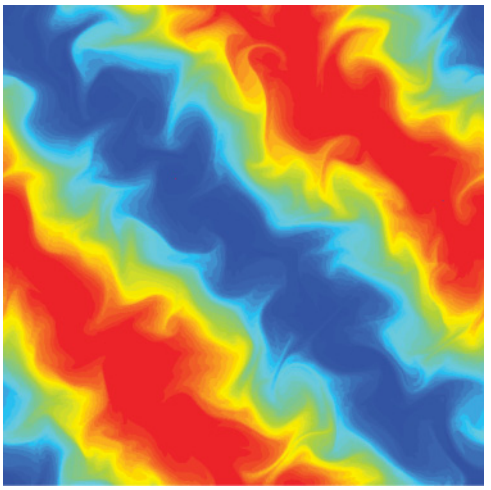

FIG. 1. (Color online) Snapshot of the carrying-capacity field $K(\mathbf{x},t)$, where blue (dark gray) and red (light gray) indicate low ($K_{\min} = 1$) and high ($K_{\max} = 2$) concentrations respectively.

fluid-ecosystem equations until the PZ system reaches a statistically steady state.

III. NUMERICAL RESULTS

In Fig. 1, we show a snapshot of the carrying-capacity field, $K(\mathbf{x},t)$, obtained after evolving Eq. (1a). Although the individual fluid particles are advected around the whole domain by the flow, the carrying-capacity field looks qualitatively similar to this throughout the time evolution, with the overall structure close to the background carrying-capacity field $K_b(\mathbf{x})$.

Figure 2 shows snapshots of the phytoplankton (top row) and zooplankton field (bottom row) after they have reached statistical equilibrium for different values of γ in the case of the linear grazing function. For the slow-mixing case ($\gamma = 0.004$), the phytoplankton field is homogeneous, showing little variation in concentration, whereas the zooplankton field has large heterogeneity. This patchiness in the zooplankton field is associated with the carrying-capacity field shown in Fig. 1. As the rate of mixing increases ($\gamma = 0.4$), greater patchiness is seen in the phytoplankton field. However, this patchiness passes a maximum value and decreases with further increases in γ. On the other hand, the zooplankton field patchiness is maximum when there is no mixing and decreases as γ increases. In Fig. 3, we show the case with Holling type III functional response, which is qualitatively similar to the linear grazing case (also, similar behavior is observed for the Holling type II case, not shown here).

The average and variance of the phyto- and zooplankton fields as a function of γ are shown in Figs. 4 and 5, respectively. Overall, there is only a very weak change in the mean concentrations with γ. However, note the nonmonotonic dependence of phytoplankton variance on γ, indicating strongest patchiness for intermediate γ values. This dependence is typical of resonance phenomena which have been observed in many systems. In fact, this phenomenon was seen in a previous study of a PZ model where resonance occurred between random fluctuations (noise) in the system and external periodic forces [31]. Here, however, the resonance is linked to the relative advection and ecosystem time scales (γ). In the following section, we analyze the governing equations in order to understand this behavior.

IV. ANALYSIS

As shown previously for this type of models (see, e.g., [20,32]), the average concentration can be calculated for the two limiting cases of fast and slow mixing, that is, large and small γ, respectively. In the simple case of $\gamma = 0$, the advection term vanishes, and by neglecting weak diffusion the steady state can be obtained as the local equilibrium:

$$G(P^*) = \frac{\mu}{\nu g}, \quad Z^* = \frac{\mu P^*}{\nu}\left(1 - \frac{P^*}{K(\mathbf{x})}\right), \tag{5}$$

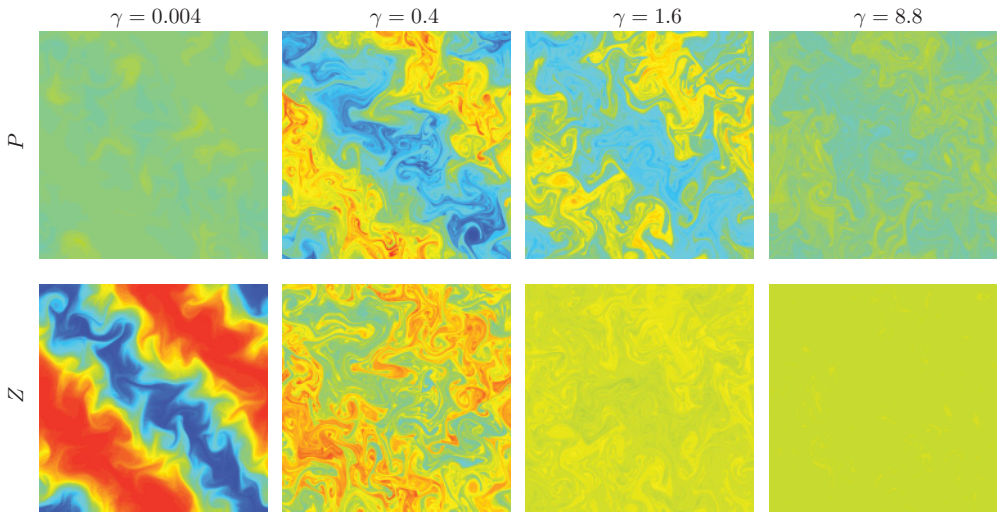

FIG. 2. (Color online) Phytoplankton (top row) and zooplankton (bottom row) fields after a statistically steady state is reached for case (i) (linear grazing function) and $\gamma = 0.004$ (first column), $\gamma = 0.4$ (second column), $\gamma = 1.8$ (third column), and $\gamma = 8.8$ (fourth column). Blue (dark gray) and red (light gray) indicate low and high concentration values respectively.

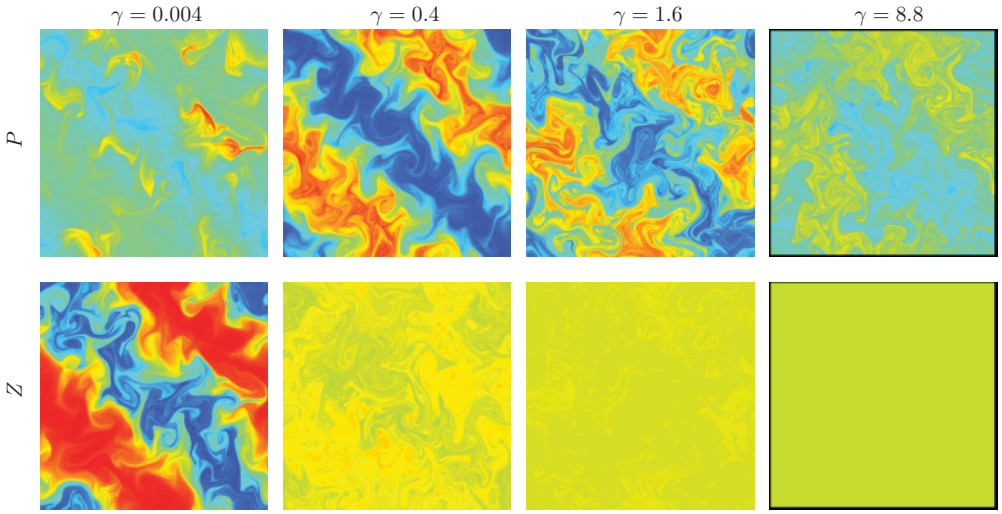

FIG. 3. (Color online) As in Fig. 2, but now for the case of Holling type III grazing function.

where the first equation implies that the phytoplankton steady state, P^*, is uniform in space and independent of the local carrying capacity, while from the second one it follows that the zooplankton field is spatially nonuniform. This is consistent with the numerical results for small γ and is a consequence of linear zooplankton mortality that results in transferring all variability in the carrying capacity to zooplankton without affecting the phytoplankton, since changes in carrying capacity are completely compensated by nonuniform grazing. In the opposite limit of fast mixing, both P and Z fields approach a spatially uniform state, and their values can be obtained from taking the average of the Eqs. (4). Since the left-hand sides vanish in the stationary state, we obtain P and Z to be the same as the average values given by (5) for the no-mixing limit. This agrees with the numerical results (Fig. 4) that show the same average total biomass in the large and small γ limits but does not give any information about what happens at intermediate values of the time-scale ratio.

Overall, it appears that there is an intermediate mixing rate for which there is maximum patchiness in the phytoplankton field. In order to better understand this phenomenon, we analyze the ecosystem equations (4) using a Lagrangian description, that is, following fluid parcels as they evolve along flow trajectories. In this framework, we replace the advection terms in Eq. (4) with a time-dependent carrying-capacity field $K(t)$ and write the PZ equations as

$$\frac{dP}{dt} = P\left(1 - \frac{P}{K(\gamma t)}\right) - gG(P)Z, \tag{6a}$$

$$\frac{dZ}{dt} = \nu gG(P)Z - \mu Z, \tag{6b}$$

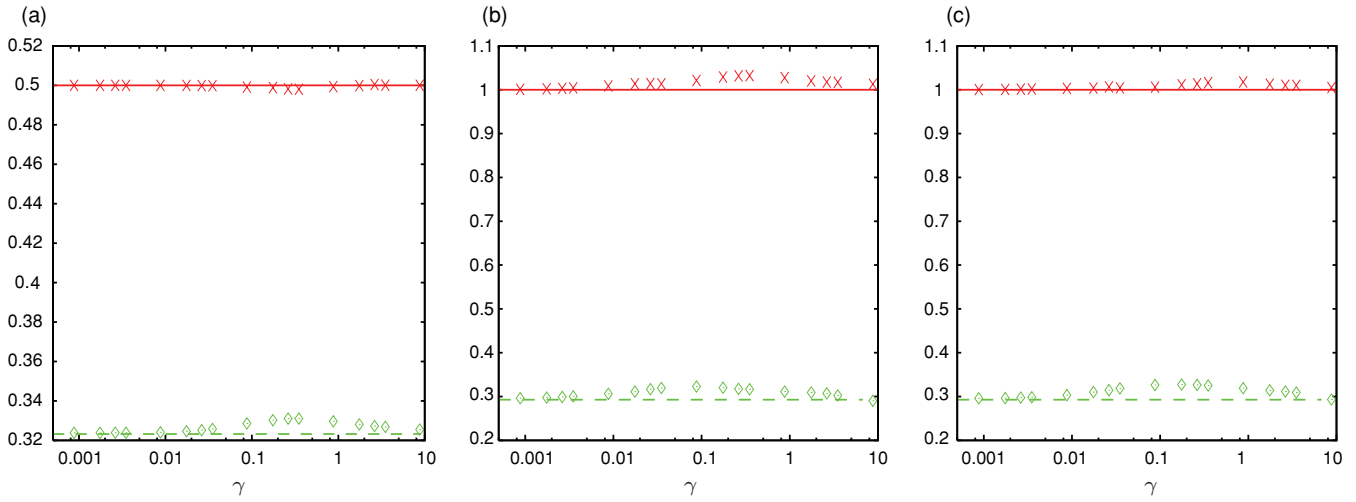

FIG. 4. (Color online) Plot of the mean of phytoplankton (red solid) and zooplankton (green dashed) vs γ (logscale) for the three different grazing functions: (a) linear, (b) Holling type II, and (c) Holling type III. The crosses and diamonds are the numerical results, whereas the solid and dashed curves are the analytical approximations discussed in Sec. IV.

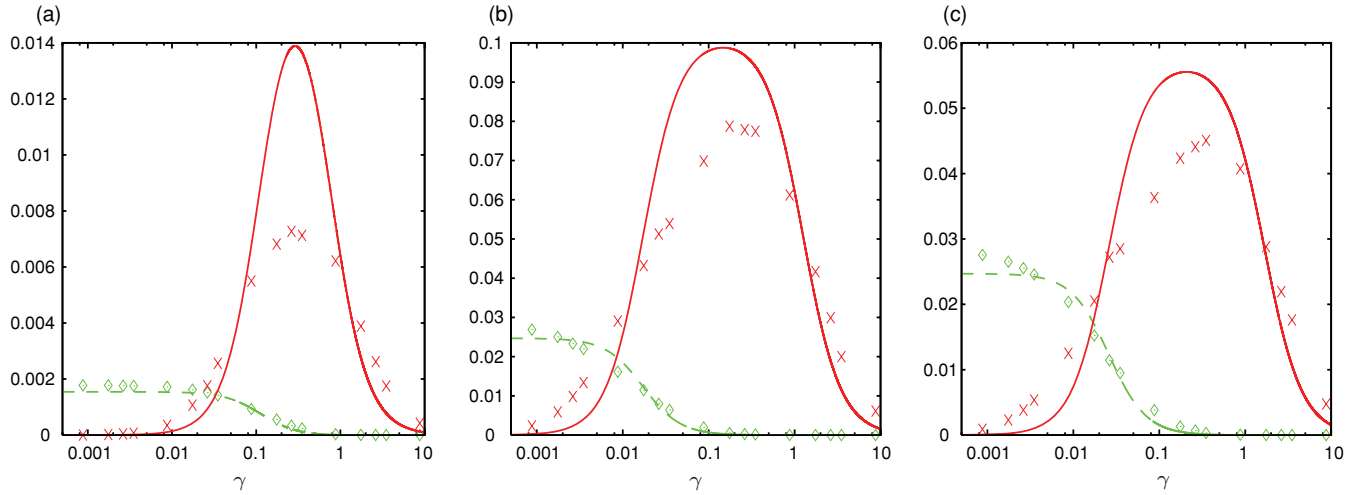

FIG. 5. (Color online) Plot of the variance of phytoplankton (crosses and red solid line) and zooplankton (diamonds and green dashed line) vs γ (logscale) for the three different grazing functions: (a) linear, (b) Holling type II, (c) and Holling type III. The symbols are the numerical results, whereas the curves are the analytical approximations discussed in Sec. IV.

where time was rescaled as $t \to t/\gamma$ and $P(t)$, $Z(t)$, and $K(t)$ are the time-dependent phytoplankton, zooplankton, and carrying-capacity concentrations in a moving parcel. In general, $K(\gamma t)$ has a chaotic aperiodic time dependence along a flow trajectory as the fluid parcels visit high- and low-carrying-capacity regions. At a given flow velocity and assuming some characteristic distance between the regions of high and low carrying capacity, there exists a characteristic time scale of the aperiodic fluctuations of K along the fluid trajectories. From previous work [20], it was found that for this turbulent flow and carrying-capacity field, the characteristic time scale T_C is related to the flow time scales by $T_C \approx 8T_F$. Thus, the carrying-capacity fluctuations can be qualitatively described by a periodic forcing $K(t) = K_0 + \delta \sin \omega t$ with frequency ω that corresponds to the time scale, $T_C = 2\pi/\omega$, which is the period of oscillation of the carrying capacity and represents the characteristic time scale for advected fluid elements to move between regions of low and high carrying capacity; thus $\omega \approx \gamma\pi/4$.

We expand the variables into an equilibrium and a time-dependent disturbance where we assume the disturbance to be small compared to the equilibrium value, that is,

$$P(t) = P_E + P'(t), \tag{7a}$$
$$Z(t) = Z_E + Z'(t), \tag{7b}$$
$$K(t) = K_E + K'(t). \tag{7c}$$

Using these in Eq. (6), we can obtain the leading-order terms for the three types of grazing functions:

$$\text{(i)}\quad P_E = \frac{\mu}{\nu g}, \quad Z_E = \frac{r\nu P_E}{\mu}\left(1 - \frac{P_E}{K_E}\right), \tag{8}$$

$$\text{(ii)}\quad P_E = \frac{\mu}{\nu g - \mu}, \quad Z_E = \frac{r\nu P_E}{\mu}\left(1 - \frac{P_E}{K_E}\right), \tag{9}$$

$$\text{(iii)}\quad P_E = \sqrt{\frac{\mu}{\nu g - \mu}}, \quad Z_E = \frac{r\nu P_E}{\mu}\left(1 - \frac{P_E}{K_E}\right). \tag{10}$$

For the disturbance terms, we obtain

$$\frac{dP'}{dt} = -2\beta_1 P' - \frac{\mu}{\nu}Z' + \frac{P_E^2}{K_E^2}K', \quad \frac{dZ'}{dt} = C_1 P'. \tag{11a}$$

$$\frac{dP'}{dt} = -2\beta_2 P' - \frac{\mu}{\nu}Z' + \frac{P_E^2}{K_E^2}K', \quad \frac{dZ'}{dt} = C_2 P'. \tag{11b}$$

$$\frac{dP'}{dt} = -2\beta_3 P' - \frac{\mu}{\nu}Z' + \frac{P_E^2}{K_E^2}K', \quad \frac{dZ'}{dt} = C_3 P' \tag{11c}$$

for the three types of grazing functions, where

$$\beta_1 = \frac{P_E}{2K_E}, \quad C_1 = \nu\mu\frac{Z_E}{P_E}, \tag{12a}$$

$$\beta_2 = \frac{1}{2}\left[\frac{P_E}{K_E}\left(1 + \frac{\mu}{\nu g}\right) - \frac{\mu}{\nu g}\right], \quad C_2 = \frac{\mu^2 Z_E}{\nu g P_E^2}, \tag{12b}$$

$$\beta_3 = \frac{1}{2}\left[1 - \frac{2\mu}{\nu g}\left(1 - \frac{P_E}{K_E}\right)\right], \quad C_3 = \frac{2\mu^2 Z_E}{\nu g P_E^3}. \tag{12c}$$

By differentiating the zooplankton disturbance equations and substituting the time derivatives for phytoplankton, the disturbance equations can be rewritten as

$$\frac{d^2Z'}{dt^2} + 2\beta_i\frac{dZ'}{dt} + \omega_i^2 = F_i \sin\omega t, \tag{13}$$

which is the well-known forced harmonic oscillator equation with natural frequency $\omega_i = \sqrt{\mu C_i/\nu}$, damping parameter β_i, and the forcing amplitude $F_i = C_i P_E^2 \delta/K_E^2$, where $i = 1, 2,$ or 3 represent the three different grazing functional types. Thus, the solutions for the disturbance equations can be obtained, and the variance of the P and Z fields are $\langle P'^2\rangle$ and $\langle Z'^2\rangle$, which are

$$\text{var}[P] = \frac{F_i^2\omega^2\langle\cos^2\omega t\rangle}{C_i^2\left[\left(\omega_i^2 - \omega^2\right)^2 + 4\beta^2\omega^2\right]}, \tag{14a}$$

$$\text{var}[Z] = \frac{F_i^2\langle\cos^2\omega t\rangle}{\left(\omega_i^2 - \omega^2\right)^2 + 4\beta^2\omega^2}. \tag{14b}$$

While the zooplankton variability decreases monotonically with the forcing frequency ω, the phytoplankton variance has a maximum when $\omega = \omega_i$ as a consequence of the resonant forcing. The forcing frequency is proportional to the time-scale ratio parameter of our model, that is, $\omega \sim \gamma$. Thus, the fact that the numerical results obtained for the turbulent flow showing increased variability of the phytoplankton field at intermediate values of γ is explained by the resonance between the Lagrangian variability of the carrying capacity and the inherent damped oscillatory dynamics of the PZ prey-predator system. The variance of the phytoplankton field in Fig. 5 clearly shows the resonance behavior as predicted by Eq. (14). The analytical model (solid curve), although not agreeing quantitatively, does capture the qualitative behavior of the full numerical solutions (crosses).

V. POWER SPECTRUM

The spatial distribution of plankton can be further characterized by its power spectrum, which shows the distribution

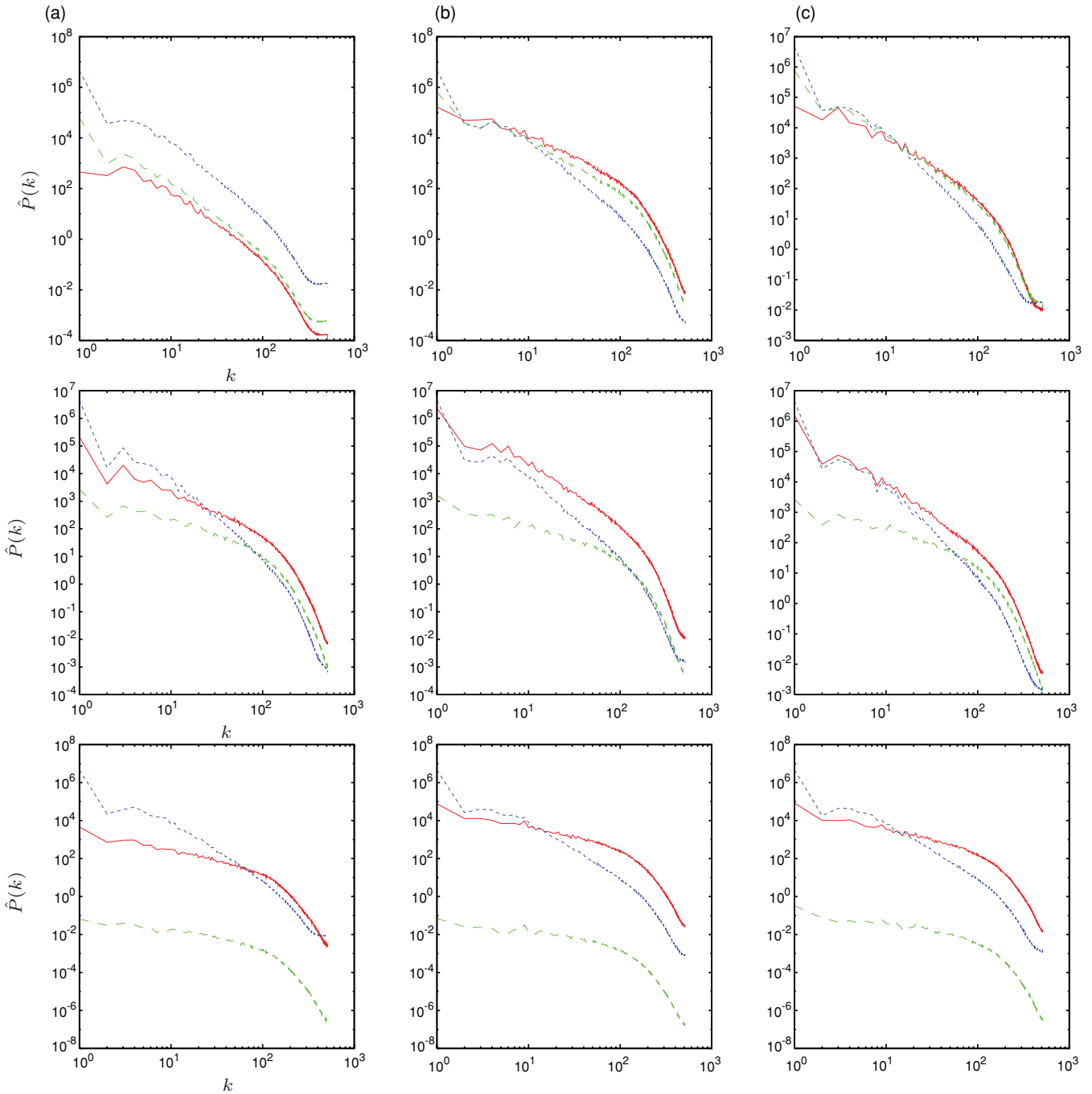

FIG. 6. (Color online) Plot of spectra of phytoplankton (red solid curve), zooplankton (green dashed curve), and carrying capacity (blue dotted curve) for the three grazing functions, linear grazing (a), Holling type II (b), and Holling type III (c), and for $\gamma = 0.004$ (top row), 0.4 (second row), and 8.8 (bottom row).

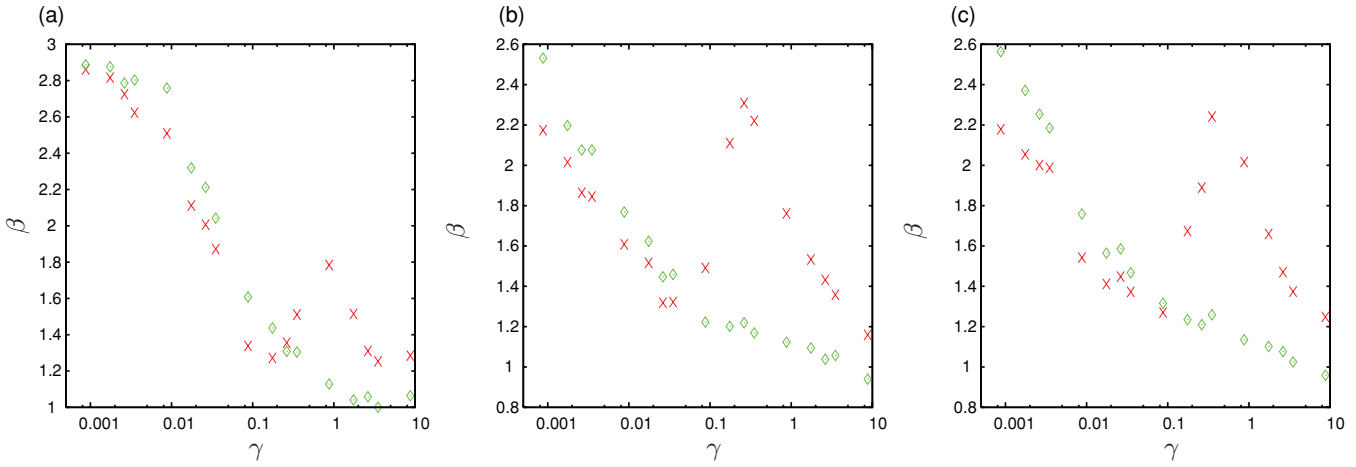

FIG. 7. (Color online) Plot of the spectral slopes of phytoplankton (red crosses) and zooplankton (green diamonds) as a function of γ (logscale) for different grazing functions. The slopes are estimated using wave numbers ranging from 10 to 80.

of variance in plankton density as a function of spatial scales. This has been often used in the analysis of both observational data and theoretical models of plankton populations (see, e.g., [16,33,34]). An important feature revealed by such spectral analysis is the presence of scaling regimes where within a certain range of length scales the spectrum follows a power law form, $\hat{P}(k) \sim k^{-\beta}$, characterized by the spectral exponent (or spectral slope) β. Alternatively, such scaling properties can also be represented by analogous quantities like the structure function defined over distances in the real space instead of the wave number space [35,36]. The spectral exponent is determined by the interplay between physical transport processes and ecosystem dynamics. In the case of inert tracers (passive scalar), there are well-established theoretical results for the value of β in different flow regimes. For the case of 2D turbulence, considered here as a model for mesoscale ocean turbulence, the spectrum of a passive scalar follows the so-called Batchelor spectrum, $\hat{P}(k) \sim k^{-1}$ [37]. For biologically active components, this is modified when the characteristic time of the ecosystem dynamics is comparable or shorter than the flow advection time scale. Previous theoretical work for chemically or biologically active tracers in chaotic and turbulent flows has shown that biological dynamics (with stable local equilibrium) leads to a spectral slope that is steeper than for a passive scalar [38–40]. The steepening is due to the damping of concentration fluctuations by the convergent ecosystem dynamics, resulting in a "leaky cascade" of tracer variance toward smaller scales with the correction term proportional to the inverse time-scale ratio, $\beta - 1 \sim \gamma^{-1}$ [20].

An interesting aspect of the observed spectrum of plankton distributions is that the zooplankton density typically has a smaller value of the spectral exponent (i.e., flatter spectrum) than the one corresponding to the phytoplankton field [3,33]. The same difference between the P and Z spectra was seen also in numerical simulations in [16], in apparent contradiction with the theory that predicts the same spectral slope for all components of a coupled ecosystem model [17]. A possible solution to this contradiction was recently suggested by the authors of [18] (see also [41]), who showed that an explicit delay term introduced in the zooplankton dynamics (as in the model of [16]), representing maturation time, can lead to different spectral slopes at certain intermediate length scales, while at small scales the slopes remain the same.

The power spectrum of the P and Z fields for the models used in our numerical simulations are shown in Fig. 6, and the estimated spectral slopes are plotted as a function of γ in Fig. 7. The slope of the zooplankton spectrum decreases monotonically with γ, consistent with the theoretical prediction for reactive scalars, approaching the Batchelor spectrum of passive scalars for large γ. The spectral slope of phytoplankton for small γ behaves in a similar way and is close to the slope for Z. This is also the case for large γ where both components follow the k^{-1} Batchelor spectrum, as expected. However, over a broad intermediate range of γ values, the phytoplankton slope has a peak where the P spectrum is significantly steeper than the Z spectrum. This is in agreement with observations of oceanic plankton distributions [33]. The steepening happens in exactly the same range of parameters where there is also an increased variance of the P field, clearly indicating a direct relationship with the resonance phenomenon described in the previous section.

Thus, our simulations show that the difference in the spectral slopes of the phyto- and zooplankton fields does not require the presence of an explicit delay in the ecosystem dynamics but can arise as a result of a resonant environmental variability along the Lagrangian trajectories, which produces an effective delay in the transfer of fluctuations through the trophic levels.

VI. DISCUSSION

We studied a PZ ecosystem in a turbulent flow and analyzed how the ecosystem changes as we varied the rate of flow relative to the biological processes by varying a dimensionless parameter, $\gamma = T_B/T_F$. Overall, while there is little change in the mean phytoplankton and zooplankton with γ, the variance of both species changes significantly. Resonance behavior is observed within the phytoplankton species with the phytoplankton patchiness reaching a maximum for an intermediate value of γ, whereas the zooplankton patchiness

decreases monotonically with γ. This phenomenon agrees qualitatively with a simplified analysis of the linearized equations, which is effectively the well-known analytical solution of the forced-damped harmonic oscillator equation. Deviations between the theoretical and numerical results are expected due to approximations made (e.g., by using a linear approximation of the ecosystem dynamics on the assumption of weak spatial heterogeneity).

We also examined the dependence of the power spectra on γ. The zooplankton spectral slope decreases monotonically with γ, similar to the behavior of a single-species model with logistic growth and nonuniform carrying capacity [20]. However, the phytoplankton spectral slope shows steepening for intermediate γ values with a local maximum occurring linked to the resonance phenomenon.

These results illustrate that the transfer of spatiotemporal heterogeneity of the environment through the trophic levels is dependent on the relative time scales of biological growth and advective transport processes. When the stirring by advection is slow in comparison to the biological population dynamics, most of the variability of the carrying capacity (e.g., due to nonuniform nutrient input) is transferred directly to the predator distribution and the prey is close to uniform. In the opposite limit of fast transport, both distributions are close to uniform and can be approximated by a mean-field description. However, the trophic transfer of variability is disrupted by the resonant interaction of the ecosystem dynamics with environmental variability, leading to an increased patchiness and steeper spectrum of phytoplankton populations.

Seasonal or regional variability of the time-scale ratio, due either to change in temperature or light conditions, mixed layer depth, or advective time scales, can lead to higher levels of patchiness when the resonance conditions are met. The models considered here do not show significant change in the average plankton concentrations when the time-scale ratio is changed. However, this may not be generally valid for more complex models of plankton population dynamics. We have shown previously that even in simple phytoplankton models the total average biomass can change as a function of the time-scale ratio even when the average carrying capacity remains constant, and this can be particularly significant when the local dynamics has a bistable character. Similar abrupt changes are likely to appear in the PZ predator-prey models when the system exhibits excitable dynamics [24] and when turbulent mixing and spatially nonuniform carrying capacity is taken into account. Further extensions considering nonlinear zooplankton mortality are also expected to lead to average biomass depending on the stirring rates.

The predicted resonance phenomenon could be detected in observations, for example, from simultaneous analysis of chlorophyll and sea surface temperature data. Our work also suggests that the difference between spectral slopes of phyto- and zooplankton can be used as an indicator of the resonance condition, which is expected to be correlated with enhanced phytoplankton patchiness, providing another testable prediction of the resonant behavior using measured distributions of phyto- and zooplankton.

ACKNOWLEDGMENTS

Support for this research has come from the Irish Research Council for Science, Engineering, and Technology and the Science Foundation of Ireland. Also we acknowledge the SFI/HEA Irish Centre for High-End Computing (ICHEC) for the provision of computational facilities and support.

[1] C. B. Field, M. J. Behrenfeld, J. T. Randerson, and P. G. Falkowski, Science **281**, 237 (1998).
[2] A. P. Martin, Philos. Trans. R. Soc. London A **363**, 2873 (2005).
[3] A. P. Martin, Prog. Oceanogr. **57**, 125 (2003).
[4] N. Blackburn, T. Fenchel, and J. Mitchell, Science **282**, 2254 (1998).
[5] R. L. Waters and J. G. Mitchell, Mar. Ecol. Prog. Ser. **237**, 51 (2002).
[6] W. M. Durham, J. O. Kessler, and R. Stocker, Science **323**, 1067 (2009).
[7] W. R. Young, A. J. Roberts, and G. Stuhne, Nature **412**, 328 (2001).
[8] C. Torney and Z. Neufeld, Phys. Rev. Lett. **99**, 078101 (2007).
[9] C. Torney and Z. Neufeld, Phys. Rev. Lett. **101**, 078105 (2008).
[10] A. Bracco, J. LaCasce, C. Pasquero, and A. Provenzale, Phys. Fluids **12**, 2478 (2000).
[11] A. Provenzale, Annu. Rev. Fluid Mech. **31**, 55 (1999).
[12] A. P. Martin, K. J. Richards, A. Bracco, and A. Provenzale, Global Biogeochem. Cycles **16**(2), 1025 (2002).
[13] M. Lévy, Lect. Notes Phys. **744**, 219 (2008).
[14] J. E. Truscott, J. Plank. Res. **17**, 2207 (1995).
[15] R. R. Sarkar, and J. Chattopadhayay, J. Theor. Biol. **224**, 501 (2003).
[16] E. R. Abraham, Nature **391**, 577 (1998).
[17] E. Hernández-García, C. López, and Z. Neufeld, Chaos **12**, 470 (2002).
[18] A. Tzella and P. Haynes, Biogeosciences **4**, 173 (2007).
[19] A. Bracco, S. Clayton, and C. Pasquero, J. Geophys. Res. **114**, C02001 (2009).
[20] W. McKiver, and Z. Neufeld, Phys. Rev. E **79**, 061902 (2009).
[21] W. McKiver, Z. Neufeld, and I. Scheuring, Nonlin. Processes Geophys. **16**, 623 (2009).
[22] C. S. Holling, Can. Entomologist **91**, 293 (1959).
[23] C. S. Holling, Can. Entomologist **91**, 385 (1959).
[24] J. E. Truscott and J. Brindley, Phil. Trans. R. Soc. London A **347**, 703 (1994).
[25] K. J. Richards and S. J. Brentnall, J. Theor. Biol. **238**, 340 (2006).
[26] P. Tabeling, Phys. Rep. **362**, 1 (2002).
[27] A. Bracco, A. Provenzale, and I. Scheuring, Proc. R. Soc. London B **267**, 1795 (2000).
[28] P. Bartello and S. Thomas, Mon. Wea. Rev. **124**, 2883 (1996).
[29] C. Temperton and A. Staniforth, Quart. J. Roy. Meteor. Soc. **113**, 1025 (1987).
[30] D. Dritschel, L. Polvani, and A. Mohebalhojeh, Mon. Wea. Rev. **127**, 1551 (1999).
[31] Q. X. Liu, Z. Jin, and B. L. Li, J. Stat. Mech. (**2008**) P05011.

[32] C. Pasquero, A. Bracco, and A. Provenzale, J. Geophys. Res. **110**, C07005 (2005).
[33] D. L. Mackas, and C. M. Boyd, Science **204**, 62 (1979).
[34] J. F. R. Gower, K. L. Denman, and R. J. Holyer, Nature (London) **288**, 157 (1980).
[35] Z. Neufeld, C. López, E. Hernández-García, and T. Tél, Phys. Rev. E **61**, 3857 (2000).
[36] E. R. Abraham, and M. M. Bowen, Chaos **12**, 373 (2002).
[37] G. K. Batchelor, J. Fluid Mech. **5**, 113 (1959).
[38] S. Corrsin, J. Fluid Mech. **11**, 407 (1961).
[39] K. Nam, T. M. Antonsen, P. N. Guzdar, and E. Ott, Phys. Rev. Lett. **83**, 3426 (1999).
[40] Z. Neufeld and E. Hernandez-Garcia, *Chemical and Biological Processes in Fluid Flows: A Dynamical Systems Approach* (Imperial College Press, London, 2009).
[41] A. Tzella and P. H. Haynes, Phys. Fluids **21**, 087101 (2009).